DESIGN OF COMBINED OPTICAL IMAGERS
USING UNMIXING-BASED HYPERSPECTRAL DATA FUSION

Naoto Yokoya[1,2] and Akira Iwasaki[1]

[1]Research Center for Advanced Science and Technology, The University of Tokyo, Japan
[2]Japan Society for the Promotion of Science, Japan
Email: yokoya@sal.rcast.u-tokyo.ac.jp

ABSTRACT

Unmixing-based hyperspectral and multispectral data fusion enables the production of high-spatial-resolution and hyperspectral imagery with small spectral errors. In this work, we present sensor design of combined optical imagers using unmixing-based data fusion, which aims to fuse hyperspectral and multispectral sensors and improve the performance of the final fused data. Owing to the degeneracy of the data cloud and additive noise, there is an optimal range in the relationship of spatial resolutions between two imagers.

Index Terms— hyperspectral and multispectral data fusion, unmixing, sensor design

1. INTRODUCTION

There are hardware limitations in the sensor design of optical imagers owing to the trade-offs between spatial resolution, spectral resolution, swath width, and signal-to-noise ratio (SNR). For instance, with the same number of detectors in the cross-track direction, if the spatial resolution is enhanced, the swath width and SNR decrease owing to the limited number of detectors and the lack of photons, respectively. Several countries are now developing hyperspectral imaging cameras as next-generation earth-observing sensors, such as HISUI, EnMAP, PRISMA, HyspIRI, and HYPXIM [1]–[5]. Generally, to maintain better SNRs than multispectral and panchromatic sensors, the spatial resolution of hyperspectral sensors is lower than that of conventional imagers. For example, HISUI, which is a Japanese next-generation earth-observing imager, consists of hyperspectral and multispectral cameras that have 30 and 5 m ground sampling distances (GSDs), respectively. PRISMA, which is the satellite remote sensing hyperspectral mission developed by Italy, is composed of hyperspectral and panchromatic imagers that have 30 and 5 m GSDs, respectively. Ideally, high resolutions both in spatial and spectral domains are desirable for optical remote sensing data to obtain better understanding of an object or phenomenon on Earth.

Unmixing-based data fusion of hyperspectral and other conventional optical sensors enables the production of high-spatial-resolution and high-spectral-resolution imagery with small spectral errors [6]. Combining several sensors using data fusion software can overcome the limitations of individual hardware. This technology may usher in a breakthrough in the sensor design of satellite optical imagers. Although individual conventional optical sensors were designed to maximize each of their performances according to their mission, data fusion can be a powerful option for sensor design, which aims to fuse several sensors and improve the performance of the final fused data. Therefore, hyperspectral data obtained by data fusion expands the possibilities of data specifications and allows a wide variety of applications. The main functions of satellite hyperspectral sensors are in the management of agricultural and forest ecosystems, disaster monitoring, water assessment, and mineral exploration [1]–[5]. The spatial resolutions of spaceborne hyperspectral sensors are approximately 30–60 m GSD, which limits satellite hyperspectral imaging applications, such as urban land cover classification of loads and buildings for hazard assessment, and crown-level tree classification in forests for ecosystem monitoring. When satellite hyperspectral imagery can be sharpened to 1–5 m GSD by fusing with multispectral and panchromatic data with a small spectral distortion, it will enable killer applications of hyperspectral remote sensing. In this work, we demonstrate a sensor design of hyperspectral and multispectral imaging system using unmixing-based hyperspectral data fusion by examining the performance of fused data with different sensor designs.

2. UNMIXING-BASED HYPERSPECTRAL AND MULTISPECTRAL DATA FUSION

The aim of hyperspectral and multispectral data fusion is to estimate unobservable high-spatial-resolution hyperspectral data from observable low-spatial-resolution hyperspectral data and high-spatial-resolution multispectral data, which have the trade-off between spectral and spatial resolutions. We consider the following assumptions for this problem:

- Multiple optical imagers are mounted on the same platform and can obtain images under the same atmo-

spheric and illumination conditions.

- Observed images are taken over the same areas and geometrically coregistered in preprocessing.

- Relative sensor characteristics, such as SRF and PSF are known.

Unmixing-based hyperspectral and multispectral data fusion, named *coupled nonnegative matrix factorization* (CNMF), is composed of alternating unmixing for two images, which is based on a linear spectral mixture model [6]. First, the algorithm starts from the unmixing of the hyperspectral data to estimate endmember spectra taking the advantage of high spectral resolution. Next, the multispectral data is unmixed after initializing the endmember spectra and the abundance fractions by using the unmixing results of the hyperspectral data. The sequential unmixing for hyperspectral data is processed after initializing the abundance fractions by using the unmixing results of the multispectral data. After that, two data are alternately unmixed until convergence and the fused data can be obtained by combining the endmember spectra and the high spatial resolution abundance maps. Fig. 1 shows the illustration of the algorithm. When the nonnegative matrix factorization (NMF) [7] is used for the unmixing process, each unmixing converges to a local minimum, and therefore the initialization is important for the unmixing. Relative spectral response functions are used to initialize the endmember spectra in the multispectral unmixing and relative point spread functions are used to initialize the abundance maps in the hyperspectral unmixing. CNMF uses the advantages of hyperspectral and multispectral data, i.e., spectral and spatial information, respectively, in other unmixing procedures to find a better local minimum. More details about the CNMF method are given in [6].

3. EXPERIMENTAL STUDY

We generate synthetic hyperspectral and multispectral datasets using several combinations of sensor specifications by simulating the trade-off of spatial resolution, spectral resolution, and SNR between hyperspectral and multispectral sensors. Let us consider a case study of HISUI/VNIR assuming a simple trade-off of sensor specifications. The hyperspectral and multispectral imagers have 1000 and 18000 pixels in the cross-track direction, respectively. As the default, the spatial resolution was set at 30 and 5 m GSDs for the hyperspectral and multispectral imagers, respectively, which are based on the specifications of HISUI. In this case, the swath widths are 30 and 90 km, respectively, and the SNRs are assumed to be 100 considering noisy bands. The multispectral imager has 4 spectral channels in the 0.45–0.52-, 0.52–0.60-, 0.63–0.69-, and 0.76–0.90-μm regions. Here, the simple principle of the specification trade-off is explained. For example, if the spatial resolution of the hyperspectral sensor is 20 m GSD and
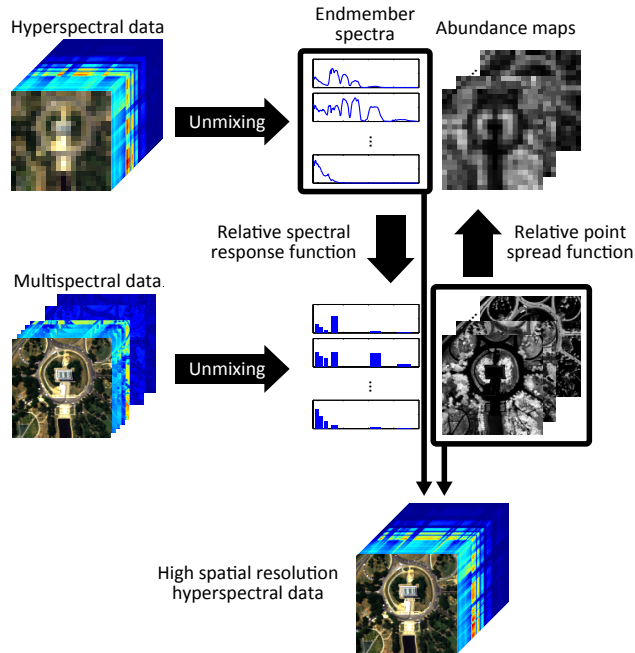
Fig. 1. Illustration of unmixing-based hyperspectral and multispectral data fusion
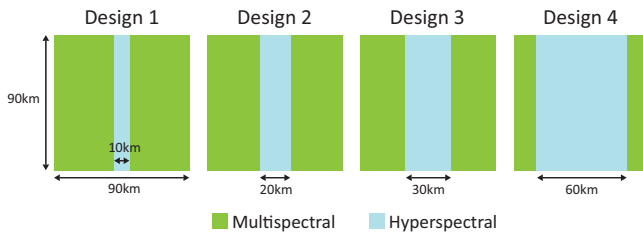
Fig. 2. Observation ranges for four sensor designs of hyperspectral (light blue) and multispectral (green) imagers.

the swath width is 20 km, the energy of photons captured by a detector per pixel is the third power of the ratio of spatial resolution, i.e., $8/27 (= (20/30)^3)$ of the energy for the 30-m-GSD hyperspectral imager, because the number of incident photons on a detector at a certain moment is proportional to the square of the ratio of the spatial resolution and the exposure time is proportional to this ratio. When we simply assume that the noise is proportional to the square root of the detected signal intensity, SNR becomes proportional to the power of 1.5, i.e., $54 (= 100 \times (20/30)^{1.5})$. Therefore, qualitatively speaking, when the spatial resolution improves, the observed area decreases and the quality of images deteriorates.

We fix the spatial resolution of the multispectral sensor and change that of the hyperspectral sensor to 10, 20, 30, and 60 m. In actual designs, HISUI, EnMAP, and PRISMA have

Fig. 3. CASI-3 images taken over (left: scene 1) forest of Tama, Tokyo in 2009 and (right: scene 2) pasture area of Motonopporo, Hokkaido in 2008.

Table 1. Specification of hyperspectral imager.

	GSD	Swath width	SNR
Design 1	10 m	10 km	19
Design 2	20 m	20 km	54
Design 3	30 m	30 km	100
Design 4	60 m	60 km	283

30 m GSD and HyspIRI has 60 m GSD. The hyperspectral sensor specifications are listed in Table 1. Fig. 2 shows the sizes of scenes observed by the two imagers. CNMF is applied to all synthetic datasets and the qualities of fused data are compared using peak signal-to-noise ratio (PSNR) and spectral angle error (SAE). An airborne hyperspectral dataset is used to generate the synthetic datasets. Two images were captured by CASI-3 with 1 m GSD taken over a forest area in Tokyo in 2009 and a pasture area of Hokkaido in 2008. A 600×600-pixel-size subimage is selected for the simulation, as shown in Fig. 3. A Gaussian blur filter is used to downgrade the spatial resolution and rectangular SRFs are used to generate multispectral images. Gaussian noise was added to satisfy the SNRs of the synthetic datasets. PSNR and SAE are used to evaluate the final fused products. The number of endmembers in CNMF is set as 20 for both images.

Fig. 4(a) and (b) show the changes in PSNR and SAE, respectively, with the GSD of the hyperspectral sensor. When the GSDs of the hyperspectral sensor are 20 and 30 m, the performance of the fused data shows the best results for both study scenes. Since the CNMF fused data is produced by multiplication of the endmember spectra obtained by hyperspectral unmixing and the abundance maps obtained by multispectral unmixing, the quality of the fused data is determined by the accuracies of two alternate unmixings. Fig. 4(c) and (d) show the RMSEs of unmixing for the hyperspectral and multispectral data, respectively. The canges in RMSE are consistent for the two scenes, and we confirmed that the combination of the accuracies of the two unmixings determines the performance of the fused data shown in Fig. 4(a) and (b).

To investigate the reason for the changes in the RMSE of
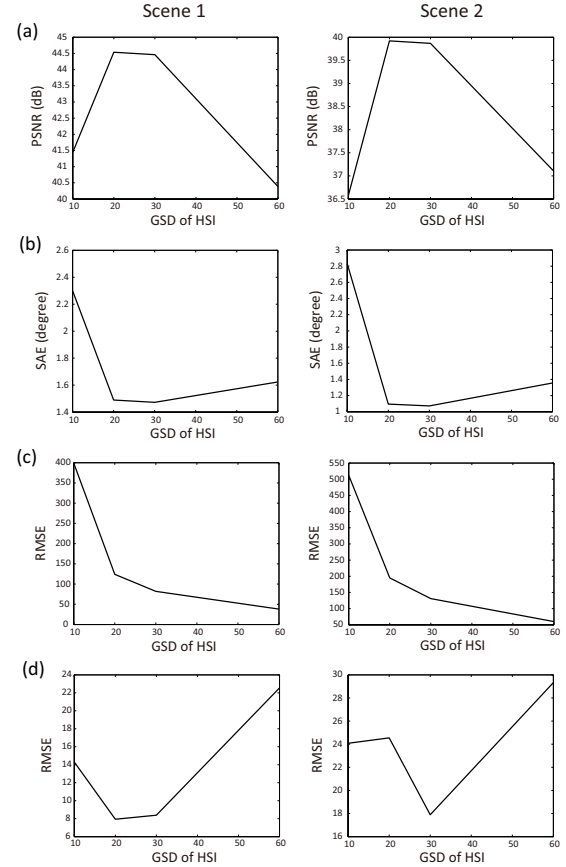
Fig. 4. (a) PSNR and (b) SAE of fused data, and RMSEs of unmixing for (c) hyperspectral and (d) multispectral data. Left column is for scene 1 and right column is for scene 2.

unmixing, Fig. 5 shows the data clouds plotted on the space defined by first and second principal components (PCs) with the first three endmembers estimated by NMF-based unmixing applied to the hyperspectral data. We compare four hyperspectral datasets with different spatial resolutions, i.e., 5, 10, 20, and 30 m GSDs, and the multispectral data with a 5 m GSD. The larger spatial resolution causes more severe degeneracy. In hyperspectral unmixing, when the number of endmembers is constant for all datasets, the data cloud with smaller spatial resolution results in larger unmixing errors owing to the more complicated structure of the data cloud and the larger noise. Therefore, the RMSE of unmixing for hyperspectral data monotonically decreases when the GSD increases. In multispectral unmixing, endmember spectra are initialized using those estimated in hyperspectral unmixing. When the GSD of a hyperspectral sensor increases, the initialized multispectral endmembers become more different from the actual endmembers in the 5 m GSD, as shown in the multispectral data cloud. In addition, when the GSD of hyperspectral data decreases, estimated endmembers can contain errors

owing to the severe noise condition of hyperspectral images. This is the reason why the change in RMSE for multispectral unmixing results in Fig. 4(d). Since there are opposite trends in the changes in RMSE for hyperspectral and multispectral data, there is an optimal range for the GSD of a hyperspectral sensor, i.e., 20–30 m in this simulation.
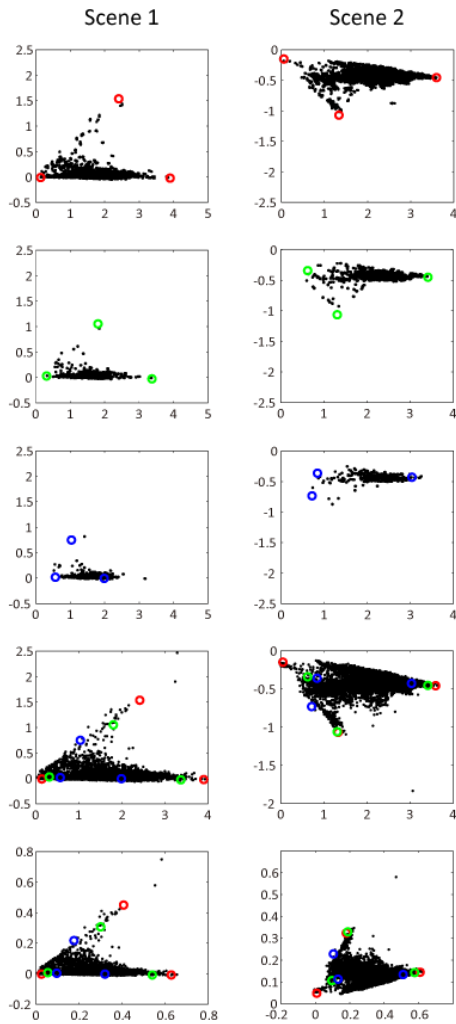
Fig. 5. From top to bottom, hyperspectral data clouds with 10, 20, 30, and 5 m GSDs and multispectral data cloud with 5 m GSD plotted on space spanned by 1st (x-axis) and 2nd (y-axis) PCs for Scene 1 (left) and Scene 2 (right). Red, green, and blue circles indicate 3 endmembers estimated from hyperspectral datasets with 10, 20, and 30 m GSDs respectively.

4. CONCLUSION

We can obtain high-spatial-resolution and high-spectral-resolution data by observing spectral information using a hyperspectral camera and spatial information using a multi-spectral camera and fusing them by hyperspectral data fusion. In this work, we presented a sensor design using combined optical imagers, which aims to use hyperspectral and multispectral data fusion and maximize the performance of fused data. We focused on examining the performance of fused data by changing the relationship of the spatial resolution between two sensors. The final performance of fused data is determined by the accuracies of two unmixings. Owing to the degeneracy of the data cloud and additive noise, there is an optimal range in the relationship of spatial resolutions between two imagers. Hyperspectral and multispectral data fusion based on unmixing contributes to the design of combined optical imagers by presenting a range of optimum design points. Combined optical imagers can usher in a major breakthrough in specifications of optical remote sensing sensors and their applications.

6. REFERENCES

[1] N. Ohgi, T. Kawashima A. Iwasaki, and H. Inada, "Japanese hyper-multi spectral mission," in *Proc. IEEE IGARSS*, pp. 3756–3759, 2011.

[2] B. Sang, J. Schubert, S. Kaiser, V. Mogulsky, C. Neumann, K.-P. Förster, S. Hofer, T. Stuffler, H. Kaufmann, A. Müller, T. Eversberg, and C. Chlebek, "The EnMAP hyperspectral imaging spectrometer: instrument concept, calibration and technologies," in *Proc. SPIE*, vol. 7086, 2008.

[3] C. Galeazzi, A. Sacchetti, A. Cisbani, and G. Babini, "The PRISMA program," in *Proc. IEEE IGARSS*, vol. 4, pp. 105–108, 2008.

[4] S. Chien, "Onboard science processing concepts for the HyspIRI mission," *IEEE Intelligent Systems*, vol. 24, no. 6, pp. 12–19, 2009.

[5] S. Michel, P. Gamet, and M. J. Lefevre-Fonollosa, "HYPXIM – a hyperspectral satellite defined for science, security and defence users," in *Proc. IEEE WHISPERS*, pp. 1–4, 2011.

[6] N. Yokoya, T. Yairi, and A. Iwasaki, "Coupled nonnegative matrix factorization unmixing for hyperspectral and multispectral data fusion," *IEEE Transactions on Geoscience and Remote Sensing*, vol. 50, no. 2, pp. 528–537, February 2012.

[7] D. D. Lee and H. S. Seung, "Learning the parts of objects by nonnegative matrix factorization," *Nature*, vol. 401, pp. 788–791, October 1999.